763. Analysis of damage characteristics for cracked composite structures using spectral element method

Hu Sun[1], Li Zhou[2]
State Key Laboratory of Mechanics and Control of Mechanical Structures
Nanjing University of Aeronautics and Astronautics
251 Mail Box, 29 Yudao Street, Nanjing 210016, China
E-mail: [1]*sunhunuaa@hotmail.com*, [2]*lzhou@nuaa.edu.cn*

(Received 22 December 2011; accepted 14 February 2012)

Abstract. Structural health monitoring of composites, due to their wide use, has attracted more attention. It is essential to study variations of structural dynamic characteristics caused by the damage. A cracked spectral element model is developed to study dynamics of cracked composite structures. Taking crack location as a boundary, the cracked composite beam is separated into two parts, which are connected by a spring. The spring, whose flexibility can be obtained by laws of fracture mechanics, is used to model axial-flexural coupling effect due to asymmetry of the crack. Calculated natural characteristics are in good agreement with the results of conventional finite element method. Lamb wave reflection and transmission at the crack location are also analyzed to verify the model. Formulations are derived to calculate power reflection and transmission of wave modes. The results indicate that power reflection/transmission ratio of a single mode is monotonic, which may provide some quantitative foundations for structural health monitoring.

Keywords: composite beam, crack, Lamb wave propagation, power reflection and transmission.

1. Introduction

Composite materials have several favorable properties, which are encouraging their use in aircraft field. With the development of composites, on-line monitoring of damage in composite structures has been an affordable technology. Lamb wave-based method is a fast and effective monitoring and plenty of work has been carried out on the experimental investigations [1, 2, 3].

Lamb wave propagation in complex structures is very complicated due to multiple reflection and mode conversion at geometrical and material features. For effectively monitoring structural health, numerical simulation is employed to extract damage features. A lot of numerical methods have also been developed for wave propagation analysis. Finite element method (FEM) [4] and finite difference method (FDM) [5, 6], owing to their own advantages, are the most common methods for wave propagation analysis. However, these two methods need a large number of calculations. Some other methods, for example, transfer function matrix [7], dynamic stiffness matrix [8], boundary element [9], strip element [10], pseudo-spectral element [11] and spectral element [12], have been developed.

Among many frequency domain methods, spectral element method (SEM), introduced by Beskos and Narayanan [13] and developed by Doyle [12], attracts wide attention because SEM needs less calculation time and memory compared with other numerical methods. SEM uses FFT to discretize time history in term of spectral amplitudes and subsequently space in wave number space. Concept of finite element nodal quantities and assembly technique is also introduced in this method. Wave propagation in isotropic and composite beams and rods has been researched [12, 14]. Meanwhile, modeling of damage is also a problem in SEM. The modeling of a delamination or horizontal crack in a beam is seen in the literatures [15, 16]. Identification of damage using SEM has also been carried out in [16, 17, 18]. Doyle [12] and Krawczuk et al [19] analyzed wave propagation in a rod and beam with a vertical fatigue crack, in which the crack was modeled as a massless spring. However, at a vertical crack, flexural and extensional wave modes must be converted from each other for asymmetry, which is not reported in the preceding papers.

The purpose of this paper is to extract some damage features for better quantitative crack identification by using SEM to model wave propagation in a composite beam with a transverse crack. The crack is modeled as a massless spring, whose flexibility can be obtained by Castigliano's theorem and laws of the fracture mechanics. Upon the displacement continuity and force equilibrium obtained from the spring, the cracked spectral element formulation can be obtained. In addition, wave propagation obtained by SEM indicates power reflection and transmission at the crack location, which may provide some foundations for identification of the crack depth.

The paper is organized as follows. In Section 2, calculation of the local flexibility of the spring is presented. The cracked spectral element formulation is derived in Section 3. Comparison of numerical results obtained by SEM and conventional FEM is provided in Section 4. Power reflection and transmission analysis obtained by SEM is studied in Section 5. Finally, in Section 6 some conclusions are drawn.

2. The local flexibility matrix at the crack location

As shown in Fig. 1(a), when a crack is present in a fiber-reinforced composite beam, the local stiffness at the crack location is weakened. Thus, the former undamaged beam can be separated into two parts, which are connected by a massless spring in Fig. 1(b) [21]. The flexibility coefficients of the spring are obtained using the Castigliano's theorem:

$$c_{ij} = \frac{\partial^2}{\partial P_i \partial P_j} \int_A d_1 \left(\sum_{n=1,3} K_{In}\right)^2 + d_2 \left(\sum_{n=1,3} K_{In}\right) K_{II2} + d_3 K_{II2}^2 dA, \text{ for } i = 1, 2, 3, \quad j = 1, 2, 3, \tag{1}$$

where A denotes the area of the crack; K_{Ii} and K_{IIi} are the stress intensity factors; P_i represent axial, shear force or bending moment; d_i can be expressed as [22]:

$$d_1 = -\frac{S_{11}}{2} \mathrm{Im}\left(\frac{\mu_1 + \mu_2}{\mu_1 \mu_2}\right), \quad d_2 = S_{11} \mathrm{Im}(\mu_1 \mu_2), \quad d_3 = \frac{S_{11}}{2} \mathrm{Im}(\mu_1 + \mu_2), \tag{2}$$

where μ_1, μ_2 are complex roots of the following equation:

$$\bar{S}_{11}\mu^4 - 2\bar{S}_{15}\mu^3 + (2\bar{S}_{13} + \bar{S}_{55})\mu^2 - 2\bar{S}_{35}\mu + \bar{S}_{33} = 0. \tag{3}$$

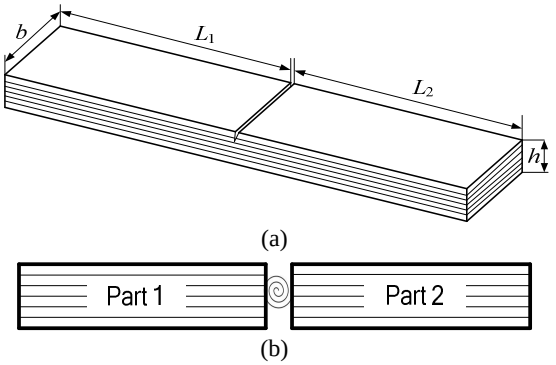

Fig. 1. A spring modeling the crack in a fiber-reinforced composite beam

$\bar{S}_{ij}$ is calculated from the following relationships:

$$\bar{S}_{11} = S_{11}m^4 + (2S_{13} + S_{55})m^2n^2 + S_{33}n^4, \tag{4a}$$

$$\bar{S}_{33} = S_{11}n^4 + (2S_{13} + S_{55})m^2n^2 + S_{33}m^4, \tag{4b}$$

$$\bar{S}_{13} = (S_{11} + S_{33} - S_{55})m^2n^2 + S_{13}(m^4 + n^4), \tag{4c}$$

$$\bar{S}_{15} = (-2S_{11} + 2S_{13} + S_{55})m^3n + (2S_{33} - 2S_{13} - S_{55})mn^3, \quad (4d)$$

$$\bar{S}_{35} = (-2S_{11} + 2S_{13} + S_{55})mn^3 + (2S_{33} - 2S_{13} - S_{55})m^3n, \quad (4e)$$

$$\bar{S}_{55} = 2(2S_{11} - 4S_{13} + 2S_{33} - S_{55})m^2n^2 + S_{55}(m^4 + n^4), \quad (4f)$$

where $m = \cos\alpha$, $n = \sin\alpha$ (α is the orientation angle). S_{ij}, denoting the mechanical property of the composites, can be calculated as:

$$S_{11} = \frac{1}{E_{11}}(1 - \nu_{13}^2 \frac{E_{33}}{E_{11}}), \quad S_{33} = \frac{1}{E_{33}}(1 - \nu_{32}^2), \quad S_{13} = -\frac{\nu_{13}}{E_{11}}(1 + \nu_{32}), \quad S_{55} = \frac{1}{G_{13}}, \quad (5)$$

whereas the mechanical parameters E_{11}, E_{33}, G_{13} and the mass density ρ can be calculated using the following formulation:

$$\rho = \rho_f V_f + \rho_m(1 - V_f), \quad E_{11} = E_f V_f + E_m(1 - V_f), \quad (6a)$$

$$E_{33} = E_m \frac{E_f + E_m + (E_f - E_m)V_f}{E_f + E_m - (E_f - E_m)V_f}, \quad \nu_{13} = \nu_f V_f + \nu_m(1 - V_f), \quad (6b)$$

$$\nu_{32} = \nu_f V_f + \nu_m(1 - V_f)\frac{1 + \nu_m + \nu_{13}E_m / E_{11}}{1 - \nu_m^2 + \nu_m\nu_{13}E_m / E_{11}}, \quad G_{13} = G_m \frac{G_f + G_m + (G_f - G_m)V_f}{G_f + G_m - (G_f - G_m)V_f}, \quad (6c)$$

where the subscript *f* denotes fiber; the subscript *m* denotes matrix; E, G, ν and ρ are the modulus of elasticity, the modulus of rigidity, the Poisson's ratio, and the mass density, respectively; and V_f denotes fiber volume fraction.

The stress intensity factors can be expressed as [23]:

$$K_{I1} = \frac{N}{bh}\sqrt{\pi\alpha}F_1\left(\frac{\alpha}{h}\right)Y_1, \quad K_{I3} = \frac{6M}{bh^2}\sqrt{\pi\alpha}F_2\left(\frac{\alpha}{h}\right)Y_2, \quad K_{II} = \frac{V}{bh}\sqrt{\pi\alpha}F_{II}\left(\frac{\alpha}{h}\right)Y_3 \quad (7)$$

where *b* and *h*, seen in Fig. 1(a), are width and height of the cross-section; α is a variable along the height direction; Y_i is corrosion function of stress intensity factors in composite beams [24]; $F_1(\alpha/h)$, $F_2(\alpha/h)$ and $F_{II}(\alpha/h)$ are expressed as [21]:

$$F_1(\alpha/h) = \sqrt{\frac{2h}{\pi\alpha}\tan\frac{\pi\alpha}{2h}}\left[0.752 + 2.02(\alpha/h) + 0.37\left(1 - \sin\frac{\pi\alpha}{2h}\right)^3\right] \Big/ \cos\frac{\pi\alpha}{2h} \quad (8a)$$

$$F_2(\alpha/h) = \sqrt{\frac{2h}{\pi\alpha}\tan\frac{\pi\alpha}{2h}}\left[0.923 + 0.199\left(1 - \sin\frac{\pi\alpha}{2h}\right)^4\right] \Big/ \cos\frac{\pi\alpha}{2h} \quad (8b)$$

$$F_{II}(\alpha/h) = \left[1.30 - 0.65(\alpha/h) + 0.37(\alpha/h)^2 + 0.28(\alpha/h)^3\right] \Big/ \sqrt{1 - \alpha/h} \quad (8c)$$

c_{ij} can be obtained from Eq. (1). The local stiffness matrix is given as follows:

$$\boldsymbol{k} = \begin{bmatrix} k_{11} & k_{12} & k_{13} \\ k_{12} & k_{22} & k_{23} \\ k_{13} & k_{23} & k_{33} \end{bmatrix} = \begin{bmatrix} c_{11} & c_{12} & c_{13} \\ c_{12} & c_{22} & c_{23} \\ c_{13} & c_{23} & c_{33} \end{bmatrix}^{-1} \quad (9)$$

3. Dynamic stiffness matrix in a cracked composite beam

Based on Timoshenko beam theory, the general displacement of a composite beam is given by:

$$U(x, y, z, t) = u(x, t) + z\psi(x, t), \quad W(x, y, z, t) = w(x, t), \quad (10)$$

where *x*-axis is the centroidal axis of the beam. $u(x, t)$ is the axial displacement of the beam in the *x*-direction; $\psi(x, t)$ is the rotation of the cross-section of the beam about the *y*-axis; $w(x, t)$ is the transverse displacement of the beam in the *z*-direction.

The axis force, bending moment, and shear force can be written as:

$$N = A_{11}u_{,x} + B_{11}\psi_{,x}, \quad V = A_{55}(w_{,x} + \psi), \quad M = B_{11}u_{,x} + D_{11}\psi_{,x}, \tag{11}$$

where $A_{55} = \sum_i \int_{z_i}^{z_{i+1}} \kappa^2 \tilde{Q}_{55} b dz$, $\left[A_{11} \quad B_{11} \quad D_{11}\right] = \sum_i \int_{z_i}^{z_{i+1}} \tilde{Q}_{11}\left[1 \quad z \quad z^2\right] b dz$, and $\left[I_0 \quad I_1 \quad I_2\right] = \sum_i \int_{z_i}^{z_{i+1}} \rho\left[1 \quad z \quad z^2\right] b dz$ (z_i and z_{i+1} are z-direction coordinates of the ith and (i+1)th plies, respectively). $\tilde{Q}_{11}$ and $\tilde{Q}_{55}$ are reduction stiffness coefficients of composite material in plane stress condition. ρ is the mass density. κ^2 is transverse shear correction factor [20].

Based on Hamilton theory, equations of wave motion can be obtained as:

$$I_0\ddot{u} + I_1\ddot{\psi} - A_{11}u_{,xx} - B_{11}\psi_{,xx} = 0, \tag{12a}$$

$$I_0\ddot{w} - A_{55}(w_{,xx} + \psi_{,x}) = 0, \tag{12b}$$

$$I_1\ddot{u} + I_2\ddot{\psi} - B_{11}u_{,xx} - D_{11}\psi_{,xx} + A_{55}(w_{,x} + \psi) = 0, \tag{12c}$$

where $\left[I_0 \quad I_1 \quad I_2\right] = \sum_i \int_{z_i}^{z_{i+1}} \rho\left[1 \quad z \quad z^2\right] b dz$.

Substituting $\left[u \quad w \quad \psi\right] = \left[U \quad W \quad \Psi\right] e^{i(kx-\omega t)}$ into Eqs. (12a)- (12c) yields as follows:

$$F_1 k^6 + F_2 k^4 + F_3 k^2 + F_4 = 0. \tag{13}$$

There exist 3 pairs of roots of wavenumber k, which represent S0, A0 and A1 wave modes. If the wavenumbers of S0 wave modes are $\pm\sqrt{\alpha}$, the roots of Eq. (13) can be obtained as:

$$k_{1,2} = \pm\sqrt{\alpha}, \tag{14a}$$

$$k_{3,4} = \pm\sqrt{-\frac{F_2 + F_1\alpha}{2F_1} + \sqrt{\left(\frac{F_2 + F_1\alpha}{2F_1}\right)^2 - \frac{\alpha(F_2 + F_1\alpha) + F_3}{F_1}}}, \tag{14b}$$

$$k_{5,6} = \mp\sqrt{-\frac{F_2 + F_1\alpha}{2F_1} - \sqrt{\left(\frac{F_2 + F_1\alpha}{2F_1}\right)^2 - \frac{\alpha(F_2 + F_1\alpha) + F_3}{F_1}}}, \tag{14c}$$

where k_1 and k_2, k_3 and k_4, k_5 and k_6 are the wavenumbers of S0, A0 and A1 wave modes.

The spectral displacement of the two elements is given by:

$$\hat{u}_i = \sum_{j=1,3,5} R_{1j}\tilde{u}_j^i e^{-ik_j x} + \sum_{j=2,4,6} R_{1j}\tilde{u}_j^i e^{ik_j(L_i - x)}, \tag{15a}$$

$$\hat{w}_i = \sum_{j=1,3,5} R_{2j}\tilde{u}_j^i e^{-ik_j x} + \sum_{j=2,4,6} R_{2j}\tilde{u}_j^i e^{ik_j(L_i - x)}, \tag{15b}$$

$$\hat{\psi}_i = \sum_{j=1,3,5} R_{3j}\tilde{u}_j^i e^{-ik_j x} + \sum_{j=2,4,6} R_{3j}\tilde{u}_j^i e^{ik_j(L_i - x)}, \tag{15c}$$

where j = 1, 2 represent Element 1 and Element 2, respectively. The time dependence term $e^{-i\omega t}$ has been suppressed here; $\tilde{u}_1$, $\tilde{u}_3$ and $\tilde{u}_5$ are incident wave spectral amplitude, and $\tilde{u}_2$, $\tilde{u}_4$ and $\tilde{u}_6$ reflected amplitude. For j = 1, 2, $R_{1j} = 1$, $R_{3j} = -\frac{A_{11}k_j^2 - I_0\omega^2}{B_{11}k_j^2 - I_1\omega^2}$, $R_{2j} = \frac{iA_{55}k_j R_{3j}}{A_{55}k_j^2 - I_0\omega^2}$.

For j = 3, 4, 5, 6, $R_{2j} = 1$, $R_{3j} = \frac{A_{55}k_j^2 - I_0\omega^2}{iA_{55}k_j}$, $R_{1j} = -\frac{(B_{11}k_j^2 - I_1\omega^2)R_{3j}}{A_{11}k_j^2 - I_0\omega^2}$.

At the left and right end of the beam, boundary conditions are:

$$\hat{u}_1|_{x=0} = \hat{u}_1^e, \quad \hat{w}_1|_{x=0} = \hat{w}_1^e, \quad \hat{\psi}_1|_{x=0} = \hat{\psi}_1^e, \quad \hat{u}_2|_{x=L_2} = \hat{u}_2^e, \quad \hat{w}_2|_{x=L_2} = \hat{w}_2^e, \quad \hat{\psi}_2|_{x=L_2} = \hat{\psi}_2^e, \tag{16}$$

where $\hat{u}_1^e$, $\hat{w}_1^e$, $\hat{\psi}_1^e$, $\hat{u}_2^e$, $\hat{w}_2^e$, $\hat{\psi}_2^e$ represent the nodal displacement.

At the crack location, force equilibrium condition can be written as:

$$\hat{N}_1 |_{x=L_1} = \hat{N}_2 |_{x=0}, \ \hat{V}_1 |_{x=L_1} = \hat{V}_2 |_{x=0}, \ \hat{M}_1 |_{x=L_1} = \hat{M}_2 |_{x=0}. \tag{17}$$

The jump conditions can be represented by:

$$\begin{bmatrix} \hat{N}_1 \\ \hat{V}_1 \\ \hat{M}_1 \end{bmatrix}_{x=L_1} = \begin{bmatrix} k_{11} & k_{12} & k_{13} \\ k_{12} & k_{22} & k_{23} \\ k_{13} & k_{23} & k_{33} \end{bmatrix} \begin{bmatrix} \hat{u}_2 |_{x=0} - \hat{u}_1 |_{x=L_1} \\ \hat{w}_2 |_{x=0} - \hat{w}_1 |_{x=L_1} \\ \hat{\psi}_2 |_{x=0} - \hat{\psi}_1 |_{x=L_1} \end{bmatrix}, \tag{18}$$

where k_{ij}, the stiffness coefficients of the spring, will be conducted in Section 1.

Substituting Eqs. (11) and (15) into Eqs. (16)-(18) yields:

$$\boldsymbol{D}_{(12\times12)} \tilde{\boldsymbol{u}}_{(12\times1)} = \boldsymbol{q}^e_{(12\times1)}, \tag{19}$$

where $\tilde{\boldsymbol{u}}_{(12\times1)} = \left\{ \tilde{u}_1^1 \ \tilde{u}_2^1 \ \tilde{u}_3^1 \ \tilde{u}_4^1 \ \tilde{u}_5^1 \ \tilde{u}_6^1 \ \tilde{u}_1^2 \ \tilde{u}_2^2 \ \tilde{u}_3^2 \ \tilde{u}_4^2 \ \tilde{u}_5^2 \ \tilde{u}_6^2 \right\}^T$, $\hat{\boldsymbol{q}}^e_{(12\times1)} = \left\{ u_1^e \ w_1^e \ \psi_1^e \ 0\,0\,0\,0\,0\,0 \ u_2^e \ w_2^e \ \psi_2^e \right\}^T$.

From Eq. (19), the following expression can be obtained as:

$$\tilde{\boldsymbol{u}}_{(12\times1)} = \boldsymbol{H}_{(12\times6)} \hat{\boldsymbol{u}}^e_{(6\times1)}, \tag{20}$$

where $\hat{\boldsymbol{u}}^e_{(6\times1)} = \left\{ \hat{u}_1^e \quad \hat{w}_1^e \quad \hat{\psi}_1^e \quad \hat{u}_2^e \quad \hat{w}_2^e \quad \hat{\psi}_2^e \right\}^T$; $\boldsymbol{H}_{(12\times6)}$, a sub-matrix of the inverse matrix of $\boldsymbol{D}_{(12\times12)}$, is given as follows:

$$\boldsymbol{H}_{(12\times6)} = \begin{bmatrix} D^{-1}_{1,1} & D^{-1}_{1,2} & D^{-1}_{1,3} & D^{-1}_{1,10} & D^{-1}_{1,11} & D^{-1}_{1,12} \\ D^{-1}_{2,1} & D^{-1}_{2,2} & D^{-1}_{2,3} & D^{-1}_{2,10} & D^{-1}_{2,11} & D^{-1}_{2,12} \\ \vdots & \vdots & \vdots & \vdots & \vdots & \vdots \\ D^{-1}_{12,1} & D^{-1}_{12,2} & D^{-1}_{12,3} & D^{-1}_{12,10} & D^{-1}_{12,11} & D^{-1}_{12,12} \end{bmatrix} \tag{21}$$

where $D^{-1}_{m,n}$ (m = 1, 2,…, 12; n = 1, 2, 3, 10, 11, 12) represents the element at the mth row and nth column in the inverse matrix of $\boldsymbol{D}_{(12\times12)}$.

Substituting Eq. (15) into Eq. (11), the nodal force vector at the left and right end of the beam can be obtained as:

$$\hat{\boldsymbol{F}}^e_{(6\times1)} = \boldsymbol{E}_{(6\times12)} \tilde{\boldsymbol{u}}_{(12\times1)}, \tag{22}$$

where the nodal force vector $\hat{\boldsymbol{F}}^e_{(6\times1)} = \left\{ \hat{\boldsymbol{N}}_1^e \quad \hat{\boldsymbol{V}}_1^e \quad \hat{\boldsymbol{M}}_1^e \quad \hat{\boldsymbol{N}}_2^e \quad \hat{\boldsymbol{V}}_2^e \quad \hat{\boldsymbol{M}}_2^e \right\}^T$.

Substituting Eq. (20) into Eq. (22) yields:

$$\hat{\boldsymbol{F}}^e_{(6\times1)} = \boldsymbol{E}_{(6\times12)} \boldsymbol{H}_{(12\times6)} \hat{\boldsymbol{u}}^e_{(6\times1)} = \boldsymbol{K}_{(6\times6)} \hat{\boldsymbol{u}}^e_{(6\times1)}, \tag{23}$$

where $\boldsymbol{K}_{(6\times6)}$ is the stiffness matrix of cracked spectral element.

4. Comparison with FEM

In order to verify the above proposed model, natural characteristic and Lamb wave propagation calculated of the cracked composite beam are studied to compare with the conventional finite element method (FEM).

4. 1. Natural characteristics

Model analysis performed with the proposed model is compared with FEM simulations. Considering a cracked composite cantilever beam in Fig. 1(a), the geometrical properties of the cracked beam are: $L_1 = L_2 = 0.5$ m, $h = 0.01$ m, $b = 0.01$ m and the crack depth $a/h = 0.3$. The properties of composite used in the numerical analysis are as follows: modulus of elasticity

E_m = 1.24 GPa, E_f = 315 GPa, modulus of rigidity G_m = 1.03 GPa, G_f = 114.8 GPa, Poisson's ratios ν_m = 0.35, ν_f = 0.23, mass densities ρ_m = 1600 kg/m^3, ρ_f = 1900 kg/m^3. The fiber volume fraction is 40%, and the ply-stacking sequence of the beam is $[0/-45/0/45/0]_s$. There are 10.000 plane strain 4-node rectangular elements in FEM, while there are just two spectral elements and a spring element in SEM. Table 1 represents natural frequencies calculated by SEM and FEM, which denotes a good agreement between the results. Second, fourth, sixth and eighth bending modes vary considerably, because wave crests of these mode shapes are at or near the crack location. Meanwhile, since nodal lines are at or near the crack, third, fifth, seventh and ninth bending modes have less change.

Table 1. Natural frequencies of a cracked composite beam calculated by SEM and FEM

Mode	Natural frequency calculated by SEM (Hz)		Natural frequency calculated by FEM (Hz)	
	Un-cracked beam	Cracked beam	Un-cracked beam	Cracked beam
First bending	14.62	14.54	14.58	14.50
Second bending	91.24	89.13	91.04	88.93
Third bending	253.87	253.86	253.35	253.34
Fourth bending	492.98	482.41	492.12	481.57
Fifth bending	805.57	805.55	804.45	804.43
Sixth bending	1186.82	1163.21	1185.69	1162.10
Seventh bending	1631.45	1631.31	1630.65	1630.51
Eighth bending	2133.70	2092.24	2133.81	2092.35
Extensional	2263.49	2253.64	2258.23	2248.40
Ninth bending	2687.83	2687.36	2689.49	2689.02

4. 2. Lamb wave propagation

Also considering a cracked composite cantilever beam in Fig. 1(a), a bending moment is loaded at the left end. The loading signal is a five-peaked narrowband wave modulated by a Hanning window, in which the wave energy is concentrated around the central frequency 50 kHz. Except that L_1 = L_2 = 1 m, other geometrical and material properties as well as ply-stacking sequence of the cracked composite beam are the same as in Section 4.1, and the crack depth a/h = 0.5.

In SEM, 65536 FFT sampling points with frequency resolution 24.414 Hz are used. In 2D plane stress FEM, a fine mesh constituting of plane strain 4-node rectangular elements as in Fig. 2. Here, the element size, 1mm×1mm, is comparable with the wavelength of the applied excitation, and the time resolution is 1 μs. In computational efficiency, the total CPU time of FEM is 550 s, while that of SEM is 6 s; the memory of FEM is 15.5 Mb, while that of SEM is 5.2 Mb. Obviously, the conventional FEM, compared with SEM, needs more computational time and memory.

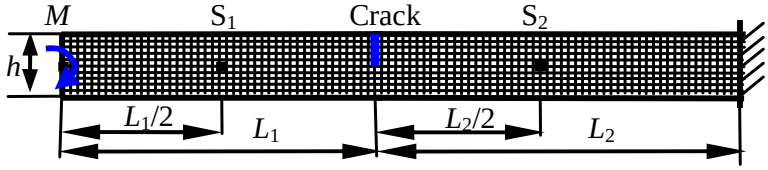

Fig. 2. The schematic of the beam modeled in FEM

The longitudinal and transverse displacements at sensor points S_1 and S_2 are given in Figs. 3(a)-(b), in which the signals are non-dimensionalized according to the incident flexural wave signal. The displacements in Figs. 3(a)-(b) denote that results obtained from SEM are consistent

with those from conventional FEM, which indicates that the proposed cracked spectral beam element is effective.

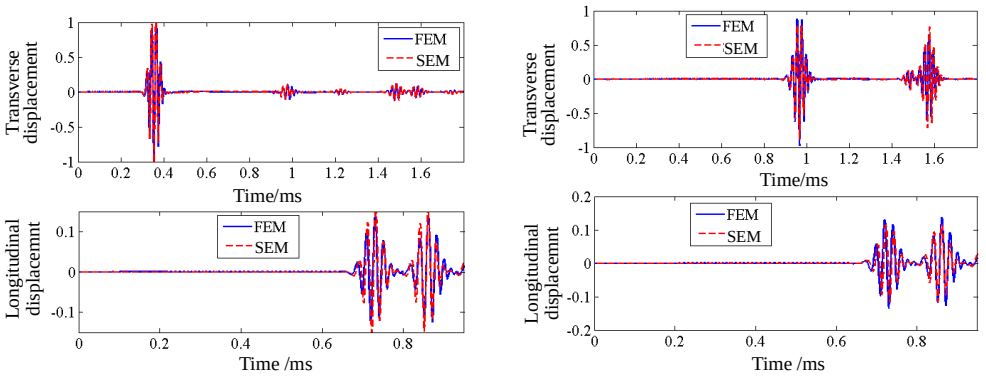

Fig. 3. Displacement of sensor: (a) point S_1; (b) point S_2

In order to demonstrate that the consistency does not depend on the location and the crack depth, further study is performed. According to crack location $L_1/(L_1+L_2)$ and the depth a/h varied from 0.2 to 0.8 in steps of 0.2 respectively, correlation coefficients between the transverse displacements at sensor point S_1 obtained from SEM and FEM are calculated to compare the similarity of the two results. The correlation coefficient between two signals $X(t)$ and $Y(t)$ is obtained as:

$$\rho_{xy} = \sqrt{\left\{\int_{t_0}^{t_1} X(t)Y(t)dt\right\}^2 \Big/ \int_{t_0}^{t_1} X(t)^2 dt \int_{t_0}^{t_1} Y(t)^2 dt} \tag{24}$$

All signals used to compare with each other are selected from 0 to 1000 μs, which contains an incident and a reflected wave pocket at least. Table 2 gives the calculated correlation coefficients varying from the location and depth of the crack. It can be observed that, although the difference between SEM and FEM increases with the varying depth, this difference is so small (the smallest correlation coefficient is 0.91) that it can be ignored. Moreover, the closer the crack is to the cantilever end, the more insensitive this difference versus the depth becomes. All the calculated correlation coefficients are greater than 0.91, which indicates that the cracked spectral element is suitable for each location or depth of the crack in reason to meet accuracy.

Table 2. Correlation coefficients between signals from SEM and FEM

a/h	$L_1/(L_1+L_2)$			
	0.2	0.4	0.6	0.8
0.2	0.99	0.99	0.99	0.98
0.4	0.99	0.98	0.98	0.98
0.6	0.98	0.97	0.98	0.98
0.8	0.91	0.94	0.96	0.98

5. Reflected and transmitted power ratios

The crack with the varying depth will reflect and transmit extensional or flexural wave with different amplitudes, which can be expressed by energy. In order to identify the crack depth, it is necessary to establish the quantitative relation between energy conversion and the depth of crack,

which will provide quantitative theoretical foundations for damage identification.

The speed of energy transport, i.e. power flow, can be expressed as the rate of work of internal forces and moments acting on a beam cross-section. Over a period T, the time-averaged power flow can be given as:

$$\hat{P} = \frac{1}{T}\int_0^T (N\dot{u} + V\dot{w} + M\dot{\phi})dt \,. \tag{25}$$

Substituting Eqs. (11) and (15) into Eq. (25), the power flow of different wave modes can be obtained as:

$$\hat{P}_1 = \lambda_1 |\tilde{u}_1|^2 \,, \quad \hat{P}_2 = \lambda_3 |\tilde{u}_3|^2 \,, \quad \hat{P}_3 = \lambda_5 |\tilde{u}_5|^2 \, H(\omega - \omega_c) \,, \tag{26}$$

where $\lambda_m = \omega[A_{11}k_m |R_{1m}|^2 + A_{55}k_m |R_{2m}|^2 + D_{11}k_m |R_{3m}|^2 + 2B_{11}k_m |R_{1m}||R_{3m}| + A_{55}|R_{2m}||R_{3m}|]/2$ (m = 1, 3, 5). $\hat{P}_1$, $\hat{P}_2$ and $\hat{P}_3$ are the power flow of S0, A0, and A1 wave modes, respectively. The Heaviside function H used signifies that the term associated with evanescent wave does not carry energy when $\omega < \omega_c$.

For the dispersive phenomenon, the whole energy is still needed to consider all the components in the whole frequency domain. Thus, the power flow can be written as:

$$\hat{P}_j = \frac{1}{4\pi^2}\int_{-\infty}^{\infty} \lambda_j(\omega)|\tilde{u}_j|^2 \, d\omega \tag{27}$$

where j = 1, 2, 3.

Similarly as in Section 4.2, considering a composite beam with geometrical properties (L_1 = L_2 = 1 m) in Fig. 2, the loading signal is also the modulated wave with the central frequency of 50 kHz. Figs. 4(a) and 4(b) give the transverse and longitudinal displacement at sensor point S_1 and S_2 when the crack depth a/h varies from 0.2 to 0.8 in steps of 0.2. The second wave mode of transverse displacement at S_1 in Fig. 4(b), i.e. reflected A0 wave mode, becomes bigger with the varying crack depth. The longitudinal displacement in Figs. 4(a) and 4(c) denotes that the reflected and transmitted S0 wave pockets both become larger when the crack is deeper. It can be observed from Fig. 4(d) that the transmitted A0 wave amplitude decreases with the increasing depth of crack.

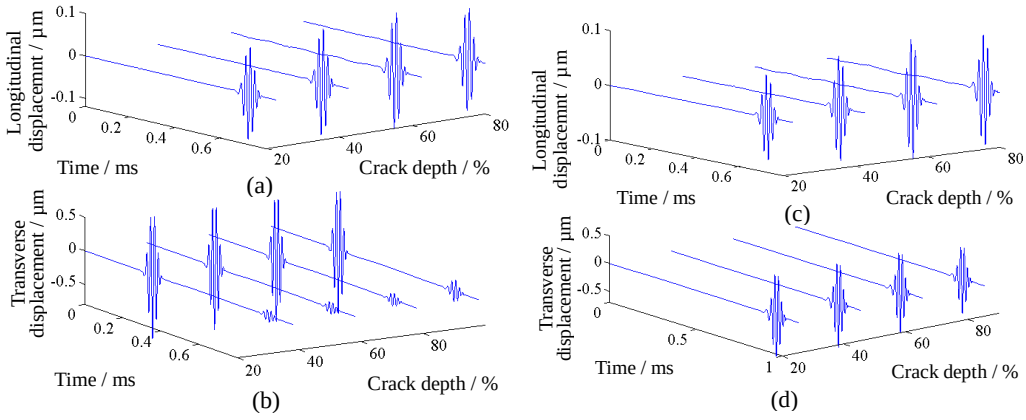

Fig. 4. Displacement of sensor versus the crack depth:
(a) longitudinal displacement at point S_1; (b) transverse displacement at point S_1;
(c) longitudinal displacement at point S_2; (d) transverse displacement at point S_2

Fig. 5 is energy conversion ratio (compared with incident wave energy) versus the crack depth of the composite beam, which is calculated by Eq. (27). Reflected energy for S0 wave is the same as transmitted one, which monotonically increases with the increasing crack depth. It also can be observed that the reflected energy of A0 wave increases from zero and will be equal to the incident wave at $a/h = 1$. Inversely, the transmitted A0 wave monotonically decreases as the crack becomes deeper and its energy ratio will be zero at $a/h = 1$. Variation of the energy is similar as that of wave amplitude. In addition, the total energy of reflected and transmitted wave modes equals the incident energy and does not vary from the crack, which indicates energy conservation and further verifies the proposed model. The monotone change of energy for each wave mode versus the crack depth indicates the possibility of its application in the quantitative damage identification.

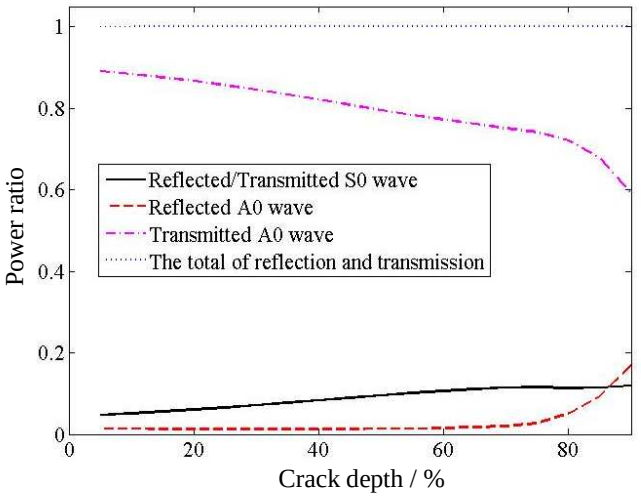

Fig. 5. Energy ratio versus the crack depth

6. Conclusions

Dynamics of a composite cracked beam is analyzed using SEM by modeling the crack as a massless spring, whose stiffness is obtained from the fracture mechanics. The cracked spectral element formulation is derived by force equilibrium and displacement continuity corresponding to the stiffness of the spring. Compared with conventional FEM, the proposed model proves to be effective in analyzing natural characteristics and wave propagation in a composite cracked beam. Power reflection and transmission with the varying crack depth is also analyzed so as to identify the crack depth. The results denote that power flows of reflected A0 wave, reflected and transmitted S0 wave all monotonically increase with the increasing crack depth, while transmitted A0 wave energy decreases. The proposed model will provide an effective tool for on-line structural health monitoring, and the present results will provide some quantitative foundations for damage identification.

Acknowledgments

This research is supported by the National Natural Science Foundation of China (under Grant No. 11172128 and Grant No. 61161120323) and the “Six Talent Peak” Project of Jiangsu Province (under Grant No. 2010-JZ-004).

References

[1] **Yu L. Y., Battai-Santoni G., Giurgiutiu V.** Shear lag solution for tuning ultrasonic piezoelectric wafer active sensors with applications to Lamb wave array imaging. International Journal of Engineering Science, Vol. 48, Issue 10, 2010, p. 848-861.

[2] **Feng Y. M., Zhou L.** Nonlinear ultrasonic test using PZT transducer for crack detection in metallic component. Journal of Vibroengineering, Vol. 13, Issue 3, 2011, p. 523-530.

[3] **Feng Y. M., Zhou L.** Combination of time reversal process and ultrasonic tomography approaches for baseline-free damage diagnosis. Journal of Vibroengineering, Vol. 13, Issue 2, 2011, p. 253-268.

[4] **Han S. J., Palazotto A. N., Leakeas C. L.** Finite element analysis of Lamb wave propagation in a thin aluminum plate. Journal of Aerospace Engineering, Vol. 22, Issue 2, 2009, p. 185-197.

[5] **Wang L., Yuan F. G.** Damage identification in a composite plate using prestack reverse-time migration technique. Structural Health Monitoring, Vol. 4, Issue 3, 2005, p. 195-211.

[6] **Meng W. J., Zhou L., Yuan F. G.** A pre-stack reverse-time migration method for multi-damage detection in composite plate. Proceedings of SPIE, Smart Structures and Materials Conference, 617444, 2006, p. 1-10.

[7] **Pao Y. H., Keh D. C., Howard S. M.** Dynamic response and wave propagation in plane trusses and frames. AIAA Journal, Vol. 37, Issue 5, 1999, p. 594-603.

[8] **Banerjee J. R., Williams F. W.** Exact dynamic stiffness matrix for composite Timoshenko beams with applications. Journal of Sound and Vibration, Vol. 194, 1996, p. 573-585.

[9] **Jin J., Quek S. T., Wan Q. G.** Wave boundary element to study Lamb wave propagation in plates. Journal of Sound and Vibration, Vol. 288, 2005, p. 195-213.

[10] **Liu G. R., Achenbach J. D.** Strip element method to analyze wave scattering by cracks in anisotropic laminated plates. ASME Journal of Applied Mechanics, Vol. 62, 1995, p. 607-613.

[11] **Ostachowic W. Z., Kudela P., Zak A., Krawczuk M.** Modeling of wave propagation in composite plates using the time domain spectral element method. Journal of Sound and Vibration, Vol. 302, 2007, p. 728-745.

[12] **Doyle J. F.** Wave Propagation in Structures. New York: Springer-Verg, 1997.

[13] **Beskos D., Narayanan G.** Dynamic response of frameworks by numerical Laplace transform. Computer Methods in Applied Mechanics and Engineering, Vol. 37, 1983, p. 289-307.

[14] **Vinod K. G., Gopalakrishnan S., Ganguli R.** Free vibration and wave propagation analysis of uniform and tapered rotating beams using spectrally formulated finite elements. International Journal of Solids and Structures, Vol. 44, 2007, p. 5875-5893.

[15] **Gangadharan R., Mahapatra D. R., Gopalakrishnan S., et al.** On the sensitivity of elastic waves due to structural damages: Time-frequency based indexing method. Journal of Sound and Vibration, Vol. 320, 2009, p. 915-941.

[16] **Krawczuk M., Palacz M., Ostachowicz W.** Wave propagation in plate structures for crack detection. Finite Elements in Analysis and Design, Vol. 40, 2004, p. 991-1004.

[17] **Nag A., Mahapatra D. R., Gopalakrishnan S.** Identification of delaminations in composite: Structural health monitoring software based on spectral estimation and hierarchical genetic algorithm. Proceedings of SPIE - The International Society for Optical Engineering, 5062, 2003, p. 720-727.

[18] **Krawczuk M., Palacz M., Zak A., et al.** Transmission and reflection coefficients for damage identification in 1D elements. Key Engineering Materials, Vol. 413-414, 2009, p. 95-100.

[19] **Krawczuk M., Palacz M., Ostachowicz W.** The dynamic analysis of a cracked Timoshenko beam by the spectral element method. Journal of Sound and Vibration, Vol. 264, 2003, p. 728-745.

[20] **Achenbach J. D.** Wave Propagation in Elastic Solids. Amsterdam: North-Holland Publishing Company, 1984.

[21] **Dimarogonas A. D., Paipetis S. A.** Analytical Methods in Rotor Dynamics. London: Applied Science Publishers, 1983.

[22] **Cowper G. R.** The shear coefficient in Timoshenko's beam theory. ASME Journal of Applied Mechanics, Series E, Vol. 33, Issue 2, 1966, p. 335-340.

[23] **Nikpur K., Dimarogonas A.** Local compliance of composite cracked bodies. Composites Science and Technology, Vol. 32, Issue 3, 1988, p. 209-223.

[24] **Bao G., Ho S., Suo Z., et al.** The role of material orthotrophy in fracture specimens for composites. Journal of Solids and Structures, Vol. 29, 1992, p. 1105-1116.